Proceedings of the
Annual Stability Conference
Structural Stability Research Council
San Antonio, Texas, March 21-24, 2017

Analyses on Seismic Behavior of Corrugated Steel Plate Shear Walls

Qiuhong Zhao[1], Junhao Sun[2], Yanan Li[3]

Abstract
Corrugated Steel Plate Shear Walls (CoSPSW) are lateral load resisting system in which corrugated steel plates are embedded inside a boundary frame, with the corrugation oriented in the horizontal or the vertical direction. Corrugated Steel Plate Shear Wall is a new type of lateral load resisting system in the family of steel plate shear walls. Compared with the unstiffened plane steel plate shear walls (SPSW), CoSPSW would have greater elastic buckling capacity, and more resistance to the gravity loads transferred to the wall panel or neatly avoid them depending on direction of the corrugation. The main focus of this paper is on the seismic behavior of CoSPSWs and comparison with SPSWs. Nonlinear push-over and cyclic analyses were conducted on a group of 3D CoSPSW and SPSW models, and parametric studies were performed with different panel and frame configuration, as well as gravity load effects. It turns out that CoSPSWs with deeper corrugation have higher lateral stiffness, lateral strength and energy dissipation than SPSWs; while CoSPSWs with shallower corrugation have higher lateral stiffness and ductility, but lower lateral strength than SPSWs. For all cases investigated, CoSPSWs have stable hysteric curves with no almost pinching, and they are much less sensitive to the influence of gravity loads or weaker boundary frames, compared with SPSWs.

1. Introduction and Background

Steel plate shear walls are excellent lateral resisting systems for multi-story and high-rise buildings, especially in highly seismic areas. Previous research has revealed that steel plate shear walls have several advantages including light weight, high lateral strength, high ductility and energy dissipation, efficient use of floor space, etc. (Driver RG et al., 1998). In the past ten years, different types of steel plate shear walls have been used in representative high-rises around the world, such as the 55 story Convention Center Hotel (2010) in Los Angeles, United States and the 75 story Jinta Tower (2010) in Tianjin China.

CoSPSWs have corrugated steel plate instead of plane plate as the wall panel, which is embedded inside a steel boundary frame. Corrugation will form “ribs” on the wall panel, and the axial and out-of-plane bending stiffness is greatly enhanced along the direction parallel to the rib,

[1] Professor, Tianjin University, <qzhao@tju.edu.cn>
[2] Engineer, China Fortune Land Development Company, < sunjunhao@cfldcn.com >
[3] Graduate student, Tianjin University,<tjuliyanan@163.com>

while the axial stiffness will become minimum along the direction perpendicular to the rib, which is called "Accordion Effects". As a result, wall panels with vertical ribs or vertical corrugation (called vertical CoSPSWs hereafter) will be able to resist the gravity loads transferred to them due to enhanced vertical buckling capacity, while wall panels with horizontal ribs or horizontal corrugation (called horizontal CoSPSWs hereafter) will neatly avoid the gravity loads transferred to them due to "Accordion Effects". In both cases, buckling of the wall panel under gravity loads will be prevented, and the panels could be conveniently erected along with the boundary frame during the construction process.

2. Finite element model and model verification

Two groups of one story, one bay SPSW and CoSPSW systems were modeled using ABAQUS, one representing the strong frame case (denoted as SC) and the other representing the weak frame case (denoted as WC). In each group, the SPSW and all CoSPSWs had the same boundary frame and wall plate thickness for comparison purpose. The following key design parameters varied for parametric studies, including 1) wall panel type (plane, sinusoidal corrugation, trapezoidal corrugation), corrugation depth (deep, shallow), corrugation direction (horizontal, vertical); 2) stiffness of boundary frame; 3) influence of gravity loads.

Boundary members in the strong frame case were designed according to AISC Design Guide 20 (Sabelli R, Bruneau M, 2006) and AISC 341-10 (2010), with wide-flange sections chosen from the US desination. Boundary members in the weak frame case were chosen as wide-flange sections with 40% lower bending stiffness than those in the strong frame case. So the beam and column section was HM500*300*11*15 (flange 300mmx15mm, web 500mmx11mm, similar to W21×68) and HW400*400*13*21 (flange 400mmx21mm, web 400mmx13mm, similar to W14×132) for the strong frame case, and HM400*300*10*16 (flange 300mmx16mm, web 400mmx10mm, similar to W16×67) and HW350*350*12*19 (flange 350mmx19mm, web 350mmx12mm, similar to W14×90) for the weak frame case, respectively.

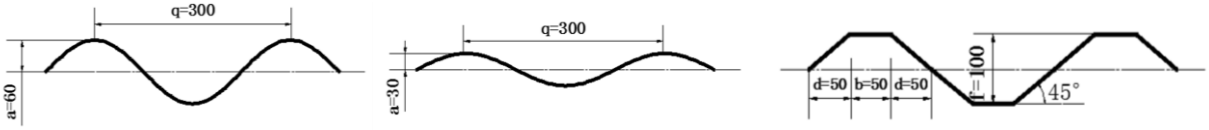

(a) Deep sinusoidal corrugation (b)Shallow sinusoidal corrugation (c) Trapezoidal corrugation

Figure 1: Profile and cross-section of corrugated panels

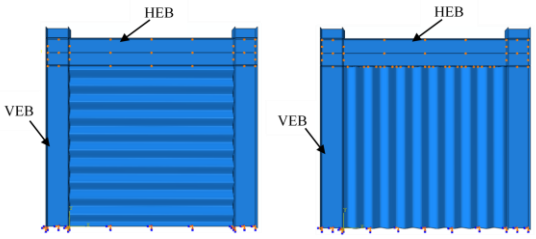

Figure 2: Geometric sketch of CoSPSWs

Wall panels all had a dimension of 3m by 3m by 5mm. The corrugated panels had a wave length of 300mm, and a wave amplitude of 60mm and 30mm, representing a deep and shallow corrugation case respectively. The vertical CoSPSW (denoted as VSW) and the horizontal CoSPSW (denoted as HSW) had the same configuration but different direction of corrugation.

The trapezoidally corrugated panel (denoted as HTW) had similar wave shape as the sinusoidally corrugated panel, with a slightly smaller wave amplitude to achieve the same fold length (length of the plate before it was corrugated). Cross-section of corrugated panels are shown in Fig. 1, and geometric sketch of the horizontal and the vertical sinusoidal CoSPSWs are showed in Fig. 2. All the FEA models are described in Table 1.

Table 1: FEA models for parametric studies

Group #	Notation	Wall type	Corrugation Wave			Wall Dimension (mm)	Boundary Section
			Direction	Length (mm)	Amplitude (mm)		
1-Strong Frame	SC-PW	Plane	——	——	——	3000*3000*5	Column HW400*400*13*21 Top Beam HM500*300*11*15
	SC-HSW-I	Sinusoidal	Horizontal	300	60		
	SC-HSW-II	Sinusoidal	Horizontal	300	30		
	SC-VSW	Sinusoidal	Vertical	300	60		
	SC-HTW	Trapezoidal	Horizontal	300	50		
2-Weak Frame	WC-PW	Plane	——	——	——		Column HW350*350*12*19 Top Beam HM400*300*10*16
	WC-HSW	Sinusoidal	Horizontal	300	60		
	WC-VSW	Sinusoidal	Horizontal	300	60		

The steel material had a yielding strength of 235Mpa for the wall panel, and 345Mpa for the boundary frame, with an elastic modulus E = 2.06×105Mpa, a Poisson's ratio v = 0.3, and a hardening modulus Eh=1/100E. All members were modeled using 4-node shell element S4R with reduced integration. Considering the high level of geometric and material nonlinearity after the wall panel buckles, seven points were used throughout the wall element thickness.

Out-of-plane initial imperfection, which may occur in plane or corrugated plates due to machining and installation, would affect the plate strength and ductility and should be properly considered in the nonlinear analyses. Due to the absence of experimental data, a common practice is to conduct eigenvalue buckling analysis, scale the major buckling modes and apply it as the initial imperfection. Initial imperfection for thin unstiffened plane plates was generally set as 1/1000 of the plate length in previous research. Considering the higher out-of-plane stiffness of corrugated plates, initial imperfection was set as 1/750 of the panel height in this study (Nie JG et al., 2013).

The column base and the bottom edge of the wall panel had a fixed boundary condition, in which all 6 degrees-of-freedom were constrained for the nodes here. In order to consider the out-of-plane bracing provided by the floor system, out-of-plane displacement of the nodes along the beam centerline and at the beam-column connection were constrained as well.

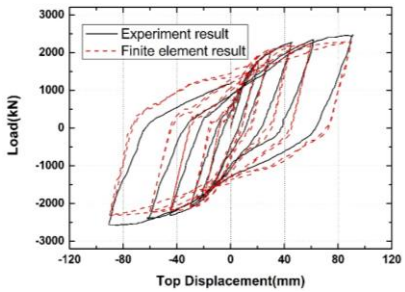

Figure 3: Model verification using Park's experimental results

In order to verify the reliability of the finite element model, one-bay, three-story SC4T specimen in Park's experiment (Park HG et al., 2007) was modeled and cyclically analyzed using ABAQUS. The load-displacement curve for the SC4T model is presented in Fig. 3, which shows a good agreement with the experimental results.

3. Nonlinear Push-over Analyses of CoSPSW and SPSW

Nonlinear push-over analyses were conducted on one SPSW (SC-PW) and two CoSPSW models, one with a wave amplitude of 60mm (SC-HSW-I), and the other with a wave amplitude of 30mm (SC-HSW-II), in order to investigate the full range of elastic and inelastic behavior of CoSPSW with deep and shallow corrugation, and compare with theoretical results.

3.1 Load-carrying Mechanism

(a)Shear yielding (b)Tension field action

Figure 4: Load carrying mechanism of corrugated and unstiffened plane plates

In a SPSW system, the unstiffened plane wall is usually very slender and prone to buckling diagonally under low levels of lateral loads. Then the wall will continue resisting lateral loads through yielding of the diagonal tensile struts across the wall, called the "tension field action", which is the main lateral load-carrying mechanism of SPSWs, as shown in Fig. 4. According to AISC Design Guide 20, lateral strength of the wall panel in SPSW is given by Eq. (1) (Sabelli R, Bruneau M, 2006).

$$V_{n,PW} = 0.5 f_y t_w L_{cf} \sin 2\alpha \tag{1}$$

where f_y is the yielding strength of the steel material; t_w is the thickness of the wall panel; L_{cf} is the clear distance between column flanges; α is the angle of inclination of the tension field from the vertical direction, permitted to be taken as 40° .

In a CoSPSW system, the elastic shear buckling stress of the wall panel will greatly increase due to corrugation, and when it is much higher than the shear yielding stress, shear yielding will happen first, which would be the load-carrying mechanism for the wall panel in this case, as shown in Fig. 4. According to the Design manual for PC bridges with corrugated steel webs (1998), for deeply corrugated web panels, the critical shear stress τ_{cr} equals the shear yielding stress τ_y, then lateral strength of the wall panel in CoSPSW with deep corrugation could be given by Eq. (2).

$$V_{n,CW} = \tau_{cr} t_w L_{cf} \tag{2}$$

where τ_{cr} is the critical shear stress that equals to the shear yielding stress; t_w is the thickness of the wall panel; L_{cf} is the clear distance between column flanges. The shear yielding stress τ_y could be determined by the Von Mises yielding criterion shown in Eq. (3).

$$\tau_y = \frac{f_y}{\sqrt{3}} \tag{3}$$

where f_y is the yielding strength of the steel material.

3.2 Nonlinear Push-over Analyses

Nonlinear push-over analyses were conducted, during which a lateral displacement was applied to a control node coupling to the nodes on the exterior column flange in the top left panel zone, and increased gradually until it reached a drift ratio of 2.5%. The lateral load versus drift ratio curves for the shear wall systems and the wall panels are shown in Fig. 5(a) and (b), respectively.

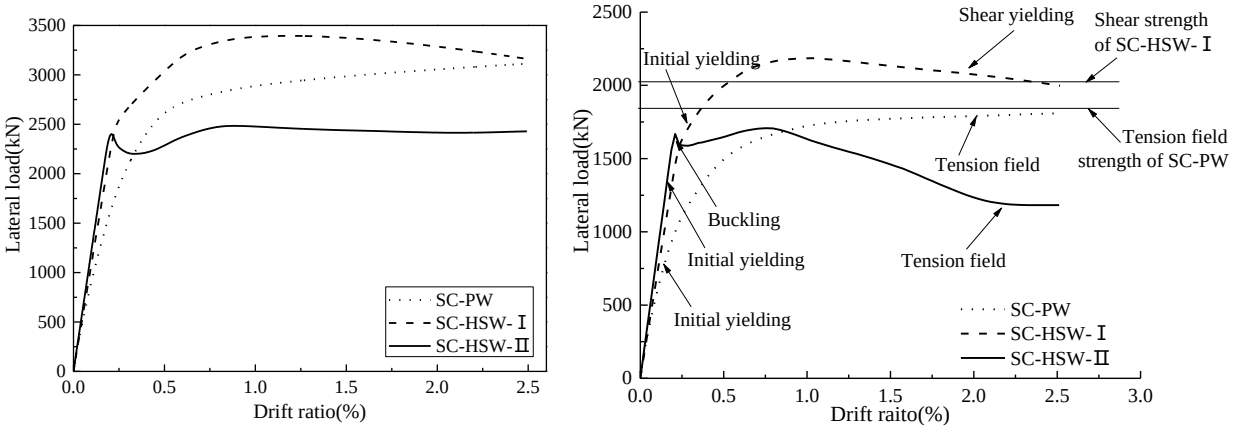

(a)Shear walls (b)Wall panels

Figure 5: Push-over curves of shear walls and wall panels

From Fig. 5, it is clear that for the SPSW (SC-PW), the wall panel started yielding at a lateral drift of 0.14%, and the tension field action gradually developed, during which more and more portion of the wall panels yielded, and the lateral strength of the wall panel was very close to the theoretical lateral strength associated with full tension field action at a lateral drift of 2%.

For the CoSPSW with deep corrugation (SC-HSW-I), the wall panel had initial yielding at a lateral drift of 0.23%, where most part of the wall panel yielded in shear, and the yielding continued until the lateral drift reached 0.4%, at which inelastic buckling occurred in the diagonal direction, and the lateral strength declined slightly, but still over the theoretical lateral strength associated with shear yielding at a lateral drift of 2%. Notice here the ultimate lateral strength of the deeply corrugated wall panel was a little higher than the theoretical lateral strength associated with shear yielding, because a bilinear material model was used in the analysis, which had a strain-hardening part.

For the CoSPSW with shallow corrugation (SC-HSW-II), the wall panel had initial yielding at a lateral drift of 0.21%, where a large part of the wall panel yielded in shear. But the wall panel did not continue yielding, instead, it had almost immediate inelastic buckling occurred in the diagonal direction, and the lateral strength had a sudden drop due to buckling, and started to form a tension field. Lateral strength of the wall panel increased slightly, but declined again after the peak, and the lateral strength of the wall panel is lower than the theoretical lateral strength

associated with full tension field action, indicating that the tension field action developed in the shallowly corrugated wall panel was not complete, which is also reflected in the stress distribution of the wall panel at a lateral drift of 2%.

Therefore, the push-over analysis shows that corrugated wall panels in CoSPSWs have quite different lateral load carrying mechanism and behavior in the elastic and inelastic stages than the SPSW. The wall panel in SPSW relies on gradual development of the tension field to resist the lateral load, and it will approach the ultimate lateral strength under a relatively large lateral drift. On the other hand, the deeply corrugated panel will tend to have the feature of a "thick" wall, for which the load-carrying mechanism is mostly shear yielding under a relatively small lateral drift, followed by inelastic shear buckling, and the lateral strength will decline as the corrugation is getting "straightened" by the inclined principal tensile stresses. The shallowly corrugated panel, however, tend to have the feature of a "thin" wall, for which the load-carrying mechanism is elastic or inelastic shear buckling. The lateral strength will drop obviously immediately after buckling, and then start to increase as the corrugation is getting "straightened" and some tension field starts to develop. The tension field will be incomplete compared to the SPSW though, which results in a lower ultimate lateral strength. More cyclic analyses are needed in order to verify the push-over results, and provide additional information on the seismic behavior of CoSPSWs such as energy dissipation and strength degradation.

4. Cyclic Analyses of CoSPSW and SPSW

Nonlinear cyclic analyses were conducted on the SPSW and CoSPSW models, in which cyclic displacements were applied to the control node. The amplitude of the displacement was increased gradually with a drift ratio of 0.25%, 0.5%, 1.0%, 1.5%, 2.0% and 2.5%, and each amplitude was repeated twice. Most of the models have reached the failure point at 2.5%, at which their lateral strength has dropped under 85% of the peak lateral strength, except for SC-PW and SC-HSW-Ⅱ, for which the cycles continued and the model reached a drift ratio of 4% and 3% respectively in the end.

4.1 Hysteretic Behavior and Backbone curves of the system

Hysteretic curves of the SPSW and CoSPSW models are shown in Fig. 6, in which the *x* axis is the drift ratio (%) and the *y* axis is reaction force at the control point (kN). It is clear that when the boundary frame and panel thickness remain the same, panel type (plane, deep corrugation, shallow corrugation) plays the most important role in the overall hysteric behavior of the CoSPSWs, while varying the corrugation direction (horizontal, vertical) or the wave shape (sinusoidal, trapezoidal) has negligible influence on the overall hysteretic behavior.

From Fig. 6(a), it is clear that hysteretic curves of the SPSW (SC-PW) have obvious pinching, which might be attributed to buckling of the wall panel and reduction of the reloading stiffness when it unloads and reloads in the opposite direction. In comparison, hysteretic curves of the CoSPSW with deep corrugation (SC-HSW-I) are plumper, especially in earlier stages, in which the wall panel has mostly shear yielding. But as the system passes the ultimate lateral strength and the wall panel starts to have inelastic buckling, the unloading stiffness starts to decline, even faster than the SPSW, and the hysteretic curves shows more pinching in the later stages. Fig. 6(a)

also shows that CoSPSW with deep corrugation has obviously higher lateral stiffness and slightly higher strength than SPSW, but the strength will decline after the peak.

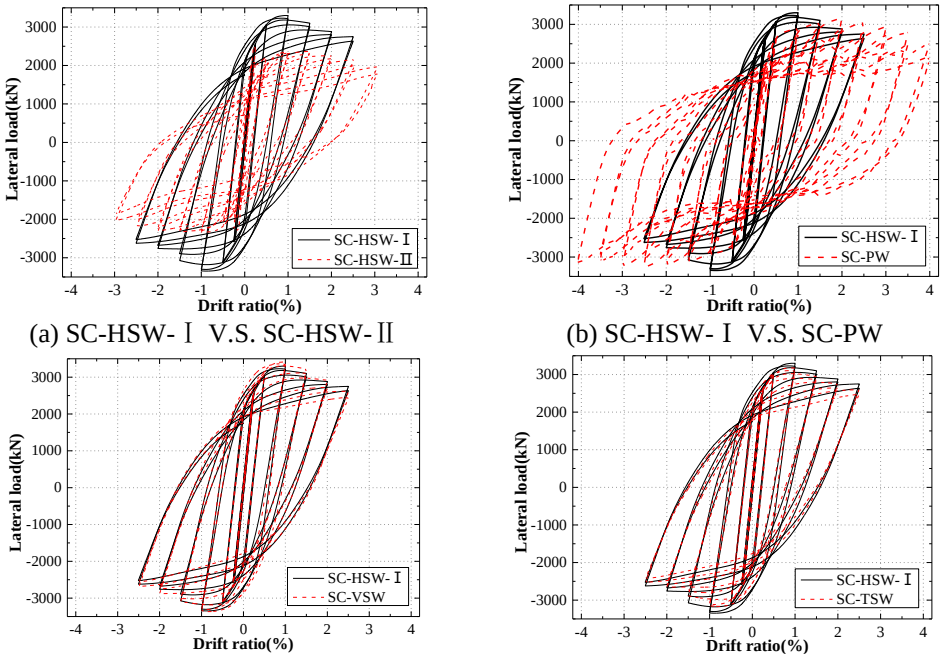

(a) SC-HSW-Ⅰ V.S. SC-HSW-Ⅱ (b) SC-HSW-Ⅰ V.S. SC-PW

(c) SC-HSW-Ⅰ V.S. SC-VSW (d) SC-HSW-Ⅰ V.S. SC-TSW

Figure 6. Hysteretic curves of shear walls with strong frame

Fig. 6(b) shows that wave amplitude plays an important role in the hysteric behavior of CoSPSWs, when the other geometric properties remain the same. The CoSPSW with higher wave amplitude and deeper corrugation has more plump hysteretic curves and higher ultimate lateral strength than the CoSPSW with lower wave amplitude and shallower corrugation (SC-HSW-II). The latter also shows an obvious dropping of the ultimate lateral strength in the early stage, and more pinching in later stages, which is associated with wall panel buckling.

Fig. 6(c) indicates that when the panel is square and no gravity loads are applied, corrugation direction has little influence on the hysteretic behavior of CoSPSWs. The vertical CoSPSW (SC-VSW) had the same elastic lateral stiffness as the horizontal CoSPSW (SC-HSW-I), and only slightly higher lateral strength and unloading stiffness. Fig. 7(d) shows that wave shape has very little influence on the hysteretic behavior of CoSPSWs as well. The trapezoidal CoSPSW (SC-HTW) had the same elastic lateral stiffness as the sinusoidal CoSPSW (SC-HSW-I), only slightly lower lateral strength and unloading stiffness.

Backbone curves are extracted from the hysteric curves of SC-PW, SC-HSW-I and SC-HSW-II in the push direction and compared with the push-over curves in the previous section, as shown in Fig. 7. It is clear that the push-over curves and the backbone curves match well in regards to the initial stiffness, lateral strength, and tendency of strength degradation, which validates the cyclic results in some sense. However, push-over analyses will underestimate the strength degradation of CoSPSWs after the peak, probably because permanent deformation of the wall panel from repeated inelastic buckling cannot be considered.

The highest displacement for the first cycle at the same lateral displacement were extracted from the hysteretic curves in both directions to form the backbone curves and the backbone curves are shown in Fig. 8. Main structural characteristics such as the initial stiffness, lateral strength and displacement at featured points on the backbone curves are shown in Table 2. Here the yielding point Y is identified with the commonly used "Equivalent area method". Point U is defined as the point at which the strength has dropped to 85% of the ultimate lateral strength, and the ductility ratio μ is defined as the ratio between the ultimate displacement Δ_u and the yielding displacement Δ_y.

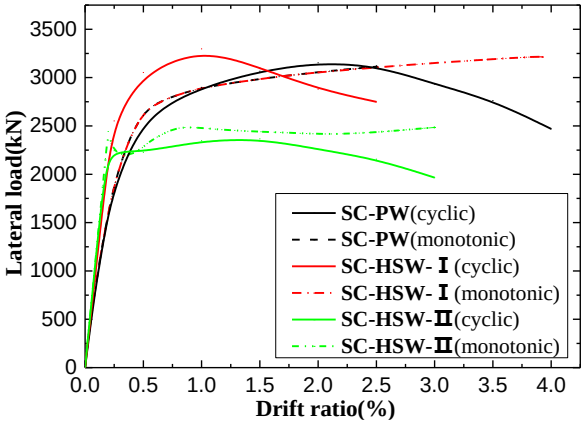

Figure 7: Comparison between push-over and backbone

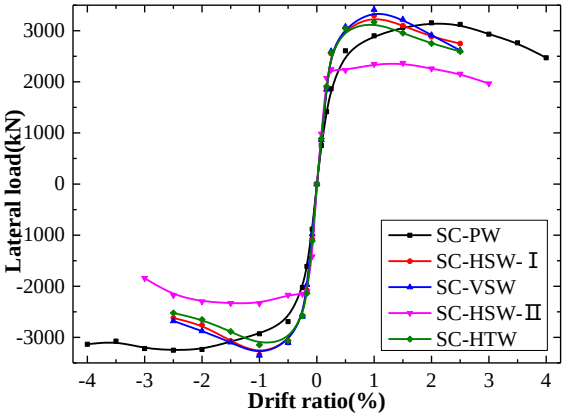

Figure 8: Backbone curves of shear walls with strong frame

Table 2: Cyclic analysis results of SPSW and CoSPSWs with strong frame

Model	Load Direction	Initial Stiffness (kN/mm)	V_y (kN)	Δ_y (mm)	V_m (kN)	Δ_m (mm)	Δ_u (mm)	μ
SC-PW	push	236	2710	24	3154	70	125-	5.2
	pull	270	2778	24	3252	88	——	——
SC-HSW-I	push	315	2869	14	3298	35	80	5.6
	pull	348	2866	14	3341	35	66	4.9
SC-HSW-II	push	353	2242	10	2367	53	98	9.8
	pull	384	2153	9	2332	53	103	11.4
SC-VSW	push	309	2956	15	3412	35	71	4.6
	pull	329	2902	14	3354	35	72	5.1
SC-HTW	push	320	2782	13	3169	35	76	6.0
	pull	356	2722	11	3148	35	68	6.0

According to Fig. 8 and Table 2, the backbone curves are basically symmetrical in the push and pull directions. The initial stiffness of CoSPSWs is always 30-50% higher than the SPSW, meaning that corrugation will effectively enhance the system lateral stiffness. CoSPSW with deep corrugation has less than 8% higher ultimate lateral strength at a 50% lower displacement, and a ductility ratio similar to the SPSW, while CoSPSW with shallow corrugation has less than 28% lower ultimate lateral strength at a 25% lower displacement, and much higher ductility ratio than the SPSW.

Similar to the hysteretic curves, the backbone curves of the horizontal CoSPSW, the vertical CoSPSW, and the trapezoidal CoSPSW are very close, and the difference could be considered

negligible. Therefore, the trapezoidal CoSPSW is no longer considered in later parametric studies,

4.2 Backbone Curves of the Wall, Frame and Lateral Strength Distribution

The "free body cut" feature of ABAQUS was utilized to obtain the lateral load resisted by the wall panel and the boundary frame at any step. Backbone curves of the wall panel and the boundary frame could then be obtained for each CoSPSW and SPSW system, and shown in Fig. 9.

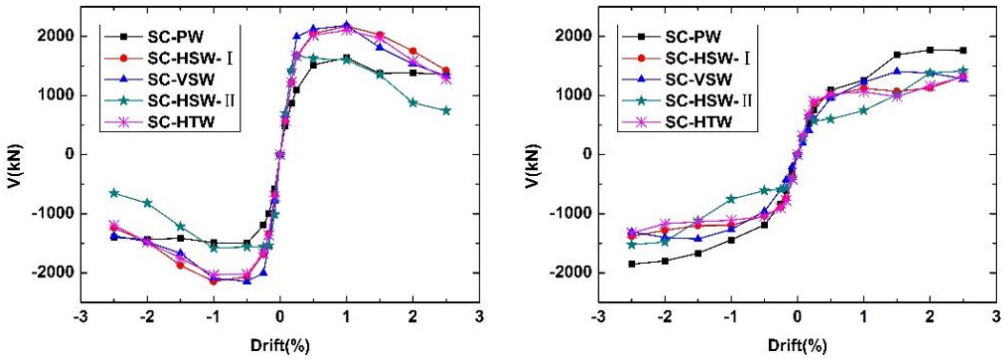

(a) Wall panels (b) Boundary frames

Figure 9: Backbone curves of wall panels and frames in shear walls with strong frame

From Fig. 9(a), it is clear that the lateral stiffness and strength of the corrugated wall panels are obviously higher than those of the plane wall panel, especially for deeply corrugated wall panels. Strength of these corrugated wall panels and the plane wall panel reaches the peak value at 1% drift and start to decline, with the corrugated panels declining faster. The lateral strength of the corrugated panels will become even lower than that of the plane wall panel after a lateral drift of 2.5%, due to the inelastic buckling and out-of-plane distortion under large drifts. Lateral strength of the shallowly corrugated wall panel will reach the peak and start to decline at a drift of 0.2%, due to buckling of the wall, and it will be 46% lower than of the plane wall panel at a drift 2.5%. This observation is consistent with the tendency shown in the push-over analyses, as well as the corresponding load-carrying mechanism of the wall panel in each system.

From Fig. 9(b), it is clear that the lateral stiffness and strength of the boundary frames are basically similar for all systems in the early stage, since they apply the same member sections, and variation in system lateral strength will be mainly in later stages. The boundary frame in the SPSW will resist more lateral loads than that in the CoSPSWs, possibly due to the anchorage needed to guarantee the tension field action in the wall panel.

The percentage of the lateral load resisted by the wall panel versus the system base shear is called the lateral load distribution factor for wall panels in this paper. The lateral load distribution curves could be deducted from the backbone curves for each CoSPSW and SPSW system, as shown in Fig. 10. As shown in Fig. 10, the lateral load distribution factor for wall panels with deep corrugation is higher than the plane wall panel, which indicates that CoSPSWs rely more on the strength of the wall panel to resist the lateral loads. This would make a more effective design, since the design shear strength of steel shear wall systems only counts the contribution of the wall currently. The lateral load distribution factor for the wall panel with

shallow corrugation is higher than the plane wall panel at the beginning but drops quickly, which means that the CoSPSW with shallow corrugation will rely more on the boundary frame to resist the lateral load, after the wall panel buckles in shear.

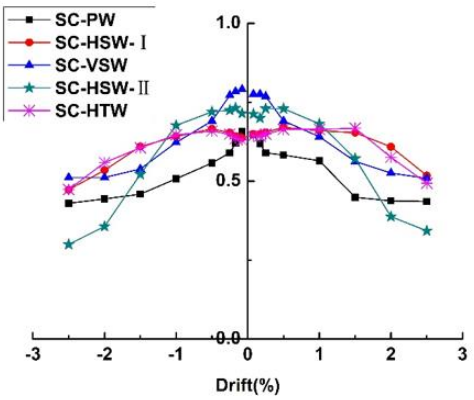

Figure 10: Lateral load distribution curves

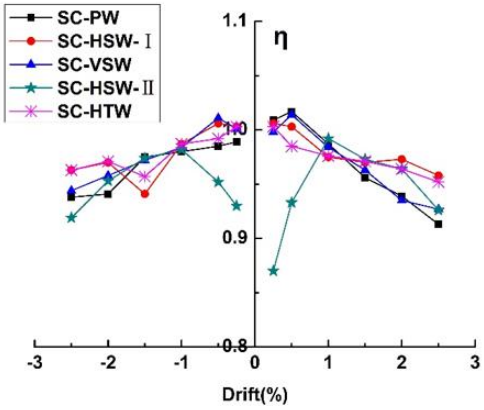

Figure 11: Lateral strength degradation

4.3 Strength degradation

Lateral strength degradation is defined as declining of the lateral strength of a structure or component with the loading cycle while the lateral displacement remains the same. The strength degradation coefficient is defined as the ratio between the shear capacity of the second cycle, and the shear capacity during the first cycle (GB50152, 1992). The strength degradation reflects the damage progression of different structural forms under cyclic load at the same displacement.

The curves of the strength degradation coefficients and the lateral drifts curves of the CoSPSWs and SPSW systems are given in Fig. 11, in which the strength degradation coefficients of the CoSPSWs and SPSW systems are generally close, varying among 0.9 to 1.0. Meanwhile, the strength coefficients of the CoSPSWs and SPSW systems basically decline linearly as the lateral drift increases. At large displacement, the tension field of the corrugated panel improved irregularly, while the tension field of plane panel extends on the opposite angles only. So the strength degradation coefficient of the CoSPSW system is apparently higher than the SPSW system. The only exception is the CoSPSW system with shallow corrugation (SC-HSW-II), of which the strength degradation is the most obvious in the first loading cycle (lateral drift of 0.25%) with the lowest strength degradation coefficient.

4.4 Energy dissipation

Energy dissipation capacity is an important parameter for evaluating the system seismic performance. Dissipated energy during a cycle is equal to the area enclosed by the hysteresis curve, and the more the enclosed area is, the better the energy dissipation capacity of the structure is. Energy dissipation capacity of a structure can also be measured by the equivalent viscous damping coefficient h_e, and higher h_e values also represent better energy dissipation capacity. Fig. 12 shows the energy dissipation performance of CoSPSWs and the SPSW during the cyclic analyses, which includes energy dissipation in each cycle, accumulated energy dissipation up to a certain cycle, and the equivalent viscous damping coefficient h_e in each cycle.

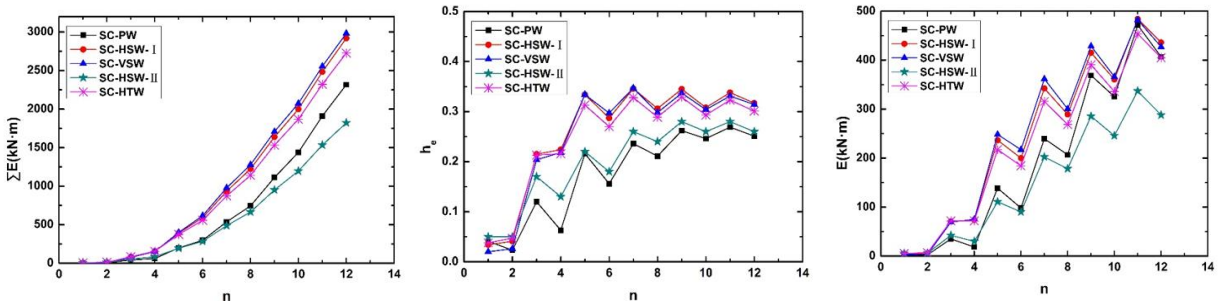

(a) Energy dissipation (b) Accumulated energy dissipation(c) Equivalent viscous damping coefficient

Figure 12: Energy dissipation of shear walls with strong frame

As illustrated in Fig. 12(a), CoSPSWs with deep corrugation (SC-HSW-I, SC-VSW, SC-HTW) have obviously higher single cycle energy dissipation than the SPSW(SC-PW), especially in the early and middle cycles when the lateral drifts are relatively small, mostly due to the higher lateral strength of these CoSPSWs in those cycles. In later cycles, as the lateral strengths of these CoSPSWs are declining and getting close to the lateral strength of the SPSW, the single cycle energy dissipation of these CoSPSWs and the SPSW are getting close as well. Fig. 12(b) shows that the accumulated energy dissipation of CoSPSWs with deep corrugation is always higher, and the total dissipated energy of these CoSPSWs is about 24% higher than that of the SPSW at cycle 12. The vertical CoSPSW dissipates slightly more energy than the horizontal CoSPSW, and the sinusoidal CoSPSW dissipates slightly more energy than the trapezoidal CoSPSW, but changing the orientation or shape of the corrugation has overall very small influence on the energy dissipation performance. Fig. 12(c) shows that the equivalent viscous damping coefficients of CoSPSWs with deep corrugation reach an average value of 0.3, and the equivalent viscous damping coefficient of SPSW reach an average value of 0.25 in the later cycles.

On the other hand, CoSPSW with shallow corrugation (SC-HSW-II) has lower single cycle energy dissipation as well as accumulated energy dissipation than the SPSW, which is more and more obvious in the later cycles. The equivalent viscous damping coefficient of SC-HSW-II is getting close to that of the SPSW in later cycles though, which might be attributed to the similar lateral load resisting mechanism, i.e. tension field action, of these two systems in later cycles.

5. Cyclic Analyses of CoSPSW and SPSW with Weak Frame

In order to investigate the influence of the boundary frame on the hysteretic behavior of corrugated steel plate shear walls as well as plane steel plate shear walls and compare the behavior, finite element models were constructed, with the same set of wall panels but reduced boundary members. The top beam section was W16×67 and the column section was W14×90, which had 40% lower bending stiffness than the boundary members of the models in the previous section.

The trapezoidal CoSPSW was not investigated, since it showed very similar hysteric behavior as sinusoidally corrugated CoSPSW in the previous section. The CoSPSW with shallow corrugation was not investigated either, since it showed lower lateral strength and energy dissipation than the SPSW in the previous section, which is expected to be even worse with a weak boundary frame. Therefore, three shear wall models were constructed with the plane wall panel, the horizontal and

the vertical sinusoidally corrugated wall panel with deep corrugation, which are then denoted as WC-PW, WC-HSW-I, and WC-VSW in this section.

5.1 Hysteretic behavior and backbone curves of the system

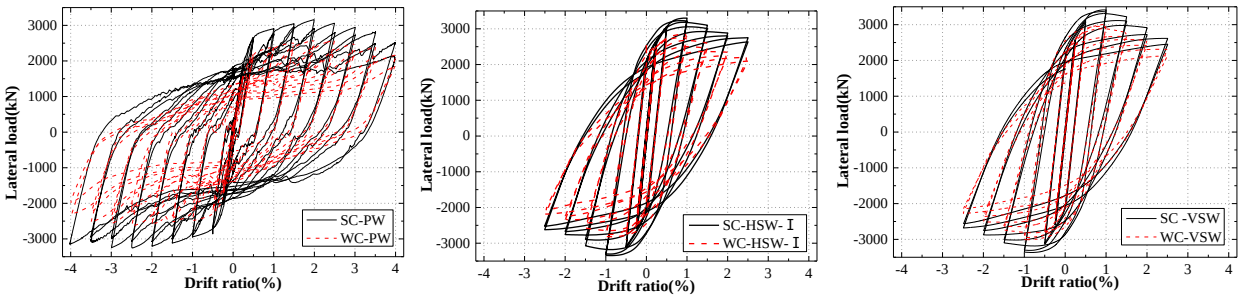

(a) SC-PW v.s. WC-PW (b) SC-HSW- I v.s. WC-HSW- I (c) SC-VSW v.s. WC-VSW

Figure 13: Hysteretic curves of shear walls with different frames

The hysteretic curves of CoSPSWs and SPSW with weak frame are compared to the hysteretic curves of corresponding systems with strong frame, as shown in Fig. 13. It can be concluded from Fig. 13 that systems with weak frame generally have similar hysteretic curves as systems with strong frame, meaning that there are no significant changes in system behavior, but with lower lateral strength. The influence of the weak frame on system behavior is more obvious for SPSW (SC-PW v.s. WC-PW) than CoSPSWs, and more obvious for the horizontal CoSPSW (SC-HSW-I v.s. WC-HSW-I) than the vertical CoSPSW (SC-VSW v.s. WC-VSW).

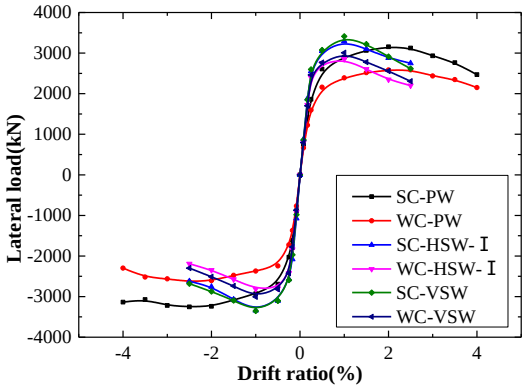

Figure 14: Backbone curves of shear walls with different frames

Backbone curves are then extracted from all hysteric curves in both directions, and shown in Fig. 14. Main structural characteristics such as the initial stiffness, lateral strength and displacement at featured points obtained from the backbone curves are shown in Table 3.

From Fig. 14 and Table 3, it is can be concluded that the initial stiffness and lateral strength of SPSW with weak frame (WC-PW) are about 11% and 18% lower than similar systems with strong frame (SC-PW), while the initial stiffness and lateral strength of CoSPSWs with weak frame (WC-HSW-I, WC-VSW) are about 5% and 13% lower than similar systems with strong frame (SC-HSW-I, SC-VSW). It seems that reducing the frame stiffness has more influence on the system lateral strength than the initial stiffness, and it affects the SPSWs to a greater extent

than the CoSPSWs. Or in other words, CoSPSWs are less sensitive to the influence of boundary frame stiffness.

Table 3: Cyclic analysis results of SPSW and CoSPSWs with weak frame

Model	Load Direction	InitialStiffness (kN/mm)	V_y (kN)	Δ_y (mm)	V_m (kN)	Δ_m (mm)	Δ_u (mm)	μ
SC-PW	push	236	2710	24	3154	70	125	5.2
	pull	270	2778	24	3252	104	——	——
WC-PW	push	211	2227	22	2585	84	133	6.0
	pull	236	2287	23	2636	95	132	5.7
SC-HSW-I	push	315	2869	14	3298	35	80	5.7
	pull	348	2866	14	3341	35	66	4.9
WC-HSW-I	push	296	2539	12	2853	34	63	5.3
	pull	316	2502	10	2812	34	65	6.2
SC-VSW	push	309	2956	15	3412	35	71	4.7
	pull	329	2902	14	3354	35	72	5.1
WC-VSW	push	293	2643	14	3008	34	68	4.9
	pull	306	2630	13	3005	34	65	5.0

When using corrugated wall instead of plane wall in the weak frame case, the initial stiffness of the system increases 40% and the lateral strength of the system increases 16%, as compared to the 30% stiffness increase and 5% strength increase in the strong frame case. Therefore, similar to the strong frame case, corrugation will increase the system stiffness to a much greater extent than the lateral strength, and this enhancement effect is more obvious when the boundary frame is weaker.

5.2 Backbone curves of the wall, frame and lateral strength distribution

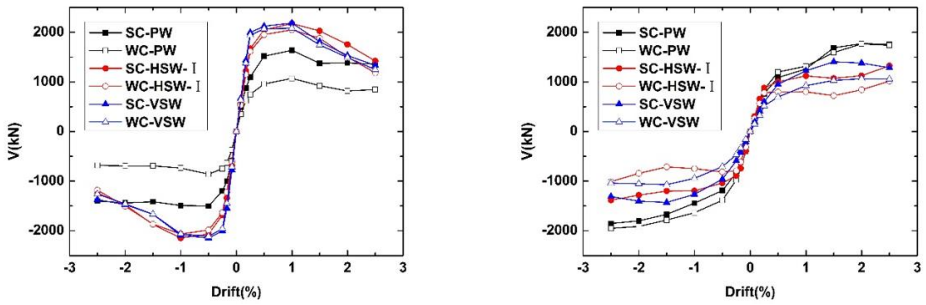

(a) Wall panels (b) Boundary frames

Figure 15: Backbone curves of wall panels and frames in shear walls with different frames

The backbone curves of the wall panel and the boundary frame are obtained for each CoSPSW and SPSW systems with weak frame, and compared to the backbone curve of the corresponding system with strong frame, as shown in Fig. 15.

As illustrated in Fig. 15, when the bending stiffness of the boundary frame is reduced 40% and a weaker frame is used, lateral strength of the wall panel in SPSW has declined 50%, but backbone curves of the boundary frame has little change, so reduction in the lateral strength of SPSW system is mainly due to the reduction in the lateral strength of its wall panel. On the contrary,

when a weaker frame is used, backbone curves of the wall panels have little change, but lateral strengths of the boundary frames have declined almost 40%, so reduction in the lateral strength of CoSPSW systems here is mainly due to the reduction in the lateral strength of its boundary frame, instead of the wall panel.

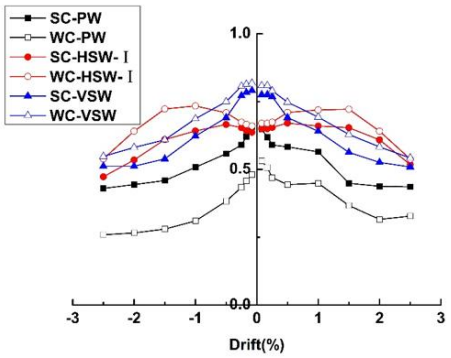

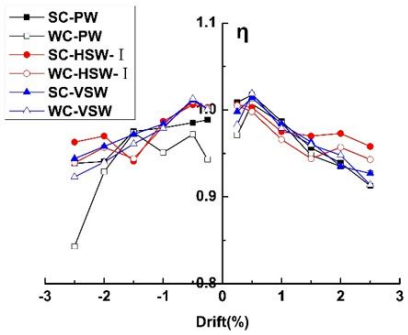

Figure 16: Lateral load distribution curves of shear walls Figure 17: Lateral strength degradation of shear walls

The lateral load distribution factor curves are deducted from the backbone curves and shown in Fig. 16. It is illustrated in Fig. 16 that when the boundary frame becomes weaker, the wall panels of CoSPSWs will tend to resist more share of the total lateral loads, while the wall panel of the SPSW will tend to resist less share of the total lateral loads. As a result, in the weak frame case, the lateral load distribution factor of the wall panel in the SPSW is much lower than those of the wall panels in CoSPSWs, which means the wall panel has not functioned effectively. This might be attributed to the fact that the weak frame can't provide sufficient constraint to the wall panel, and the tension field action of the wall panel in the SPSW with weak frame cannot develop completely, as compared to the strong frame case.

5.3 Strength degradation

Fig. 17 shows the lateral strength degradation of CoSPSWs and SPSWs with different frames. It can be seen that the fluctuation of the lateral strength degradation curves is very small, and the strength degradation coefficients are mostly above 0.9, except for the SPSW with weak frame model (WC-PW) in the reverse loading, in which the strength degradation coefficient is under 0.85 at a lateral drift of 2.5%.

5.4 Energy dissipation

Fig. 18 shows the accumulated energy dissipation of CoSPSWs and SPSWs with different frames. Generally speaking, CoSPSWs still have higher accumulated energy dissipation than the SPSW in the weak frame case, which is similar to the strong frame case. When the boundary frame becomes weaker, accumulated energy dissipation has decreased 25% for the SPSW (WC-PW), 22% for the horizontal CoSPSW (WC-HSW-I), and 14% for the vertical CoSPSW (WC-VSW), respectively. It can be concluded that reducing the frame stiffness will result in reduction of system energy dissipation, and it will affect the SPSW and the horizontal CoSPSW more than the vertical CoSPSW.

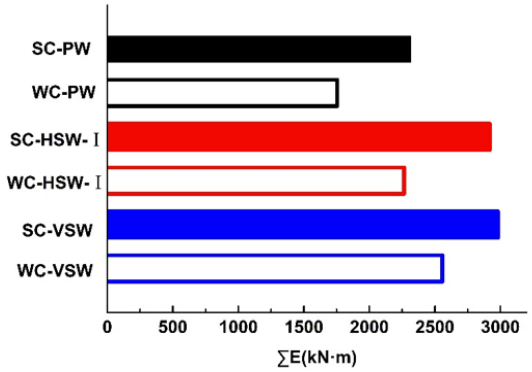

Figure 18: Accumulate energy dissipation of shear walls with different frames

6. Cyclic Analyses of CoSPSW and SPSW with Gravity Loads

In order to investigate the influence of gravity loads on the hysteretic behavior of CoSPSW and SPSW, cyclic analyses were conducted with the consideration of gravity load effects on the SPSW(SC-PW), the horizontal CoSPSW with deep corrugation (SC-HSW-I), and the vertical CoSPSW (SC-VSW). The trapezoidal CoSPSW and the horizontal CoSPSW with shallow corrugation (SC-HSW-II) were not investigated for the same reason as in the previous section.

6.1 Hysteretic behavior and backbone curves of the system

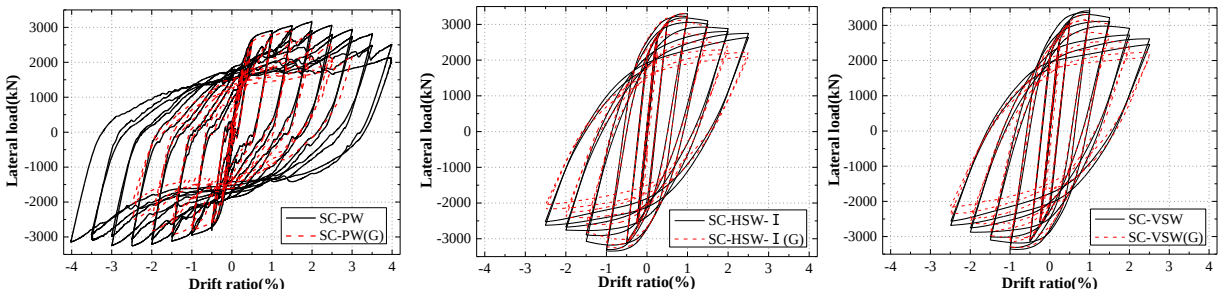

(a) SC-PW (b) SC-HSW- I (c) SC-VSW

Figure 19: Hysteretic curves of shear walls with and without gravity loads

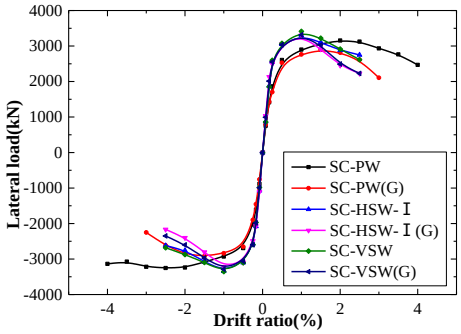

Figure 20: Backbone curves of shear walls with and without gravity loads

The hysteretic curves of SC-PW, SC-HSW-I and SC-VSW with gravity loads are plotted in Fig. 19 and compared with the hysteretic curves of the same set of models without gravity loads. It is

clear that gravity loads will affect the system hysteretic behavior by causing more pinching, faster strength deteriorating after the peak, and reduction in the unloading stiffness, and the influence is more obvious for the SPSW than CoSPSWs, since the unstiffened wall panel is easier to buckle under gravity loads.

Table 4: Cyclic analysis results of SPSW and CoSPSWs with gravity loads

Model	Load Direction	Initial Stiffness (kN/mm)	V_y (kN)	Δ_y (mm)	V_m (kN)	Δm (mm)	Δu (mm)	μ
SC-PW	push	236	2710	24	3154	70	125	5.2
	pull	270	2778	24	3252	104	——	——
SC-PW(G)	push	239	2558	20	2895	53	88	4.4
	pull	243	2653	18	2924	53	86	4.8
SC-HSW-I	push	315	2869	14	3298	35	80	5.7
	pull	348	2866	14	3341	35	66	4.9
SC-HSW-I(G)	push	356	2873	15	3299	35	57	3.8
	pull	346	2708	12	3219	35	56	4.7
SC-VSW	push	309	2956	15	3412	35	71	4.7
	pull	329	2902	14	3354	35	72	5.1
SC-VSW(G)	push	337	2851	14	3314	35	59	4.2
	pull	327	2852	14	3287	35	61	4.5

Backbone curves extracted from the hysteric curves and compared with the backbone curves of the same set of models without gravity loads, as shown in Fig. 21. Main structural characteristics such as the initial stiffness, lateral strength and displacement at featured points obtained from the backbone curves are shown in Table 4. It can be concluded that gravity loads have negligible influence on the initial stiffness of the SPSW, but decrease its lateral strength by about 10%, while gravity loads have almost no influence on the lateral strength of the CoSPSWs, but increase their initial stiffness by about 10%.

When using corrugated wall instead of plane wall and considering gravity load effects, the initial stiffness of the system increases almost 50% and the lateral strength of the system increases 14%, as compared to the 30% stiffness increase and 5% strength increase without considering gravity load effects. Therefore, corrugation will more obviously increase the system stiffness as well as the lateral strength, when gravity loads from the rest of the building are transferred to the wall panels in the steel shear wall system.

6.2 Backbone curves of the wall, frame and lateral strength distribution

The backbone curves of the wall panel and the boundary frame are obtained for each CoSPSW and SPSW systems with gravity load effects, and compared to the backbone curve of the corresponding system without gravity load effects, as shown in Fig. 21.

As illustrated in Fig. 21, gravity loads have almost no influence on the initial stiffness and lateral strength of the wall panel, but they will affect the panel behavior in later stages after the peak. Wall panels with gravity loads applied on them will have a faster strength deterioration after the peak, which is the most prominent in the SPSW, and the least in the vertical CoSPSW.

Gravity loads also tend to have little influence on the backbone curves of the frames, with only a slight reduction in the frame strength in the SPSW. Overall, the CoSPSWs are less sensitive to the gravity load effects, especially for the vertical CoSPSW.

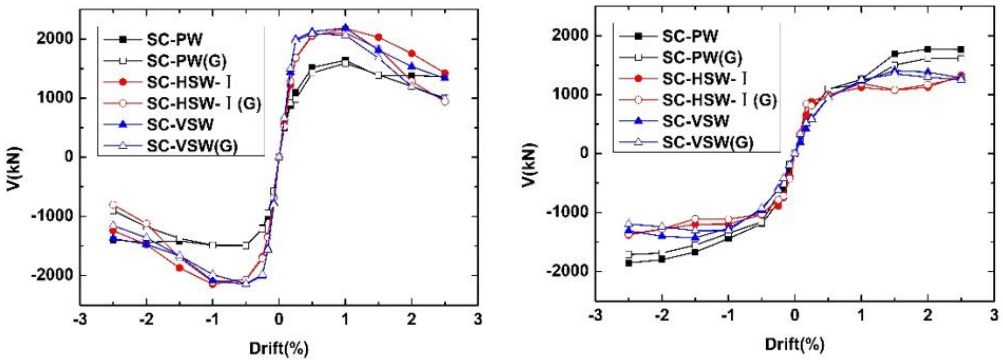

(a) Wall panels (b) Boundary frames

Figure 21: Backbone curves of wall panels and frames of shear walls with and without gravity loads

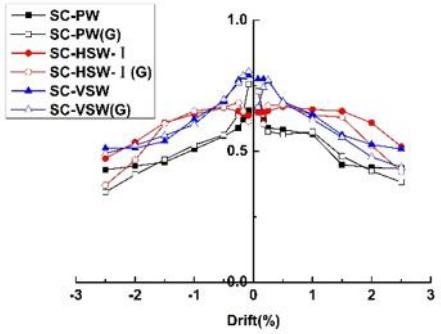

Figure 22: Lateral load distribution curves of shear walls

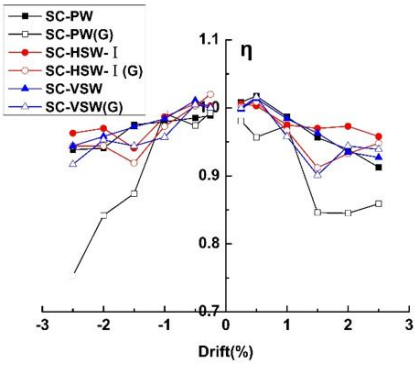

Figure 23: Lateral strength degradation of shear walls

The lateral load distribution factor curves are deducted from the backbone curves and shown in Fig. 22. It is illustrated that gravity loads have almost no influence on the lateral load distribution between the wall panel and the frame either, except for the late stages in which the panel share of the lateral loads start to decline, and more lateral loads are resisted by the frame, when the lateral drift is beyond 1%.

6.3 Strength degradation

The curves of the strength degradation coefficients and the lateral drifts curves of the CoSPSWs and SPSW systems under gravity loads or not are given in Fig. 23, in which the strength degradation coefficients of the CoSPSWs and SPSW systems are generally close, varying between 0.7 to 1.0. Meanwhile, the strength coefficients of the CoSPSWs and SPSW systems basically decline linearly as the lateral drift increases. At large displacement, corrugated panel has various extensions, and the tension field of plane panel extends on the opposite angles only. It can be seen that the lateral strength degradation becomes more significant for shear walls under gravity loads, especially for SPSW.

6.4 Energy dissipation

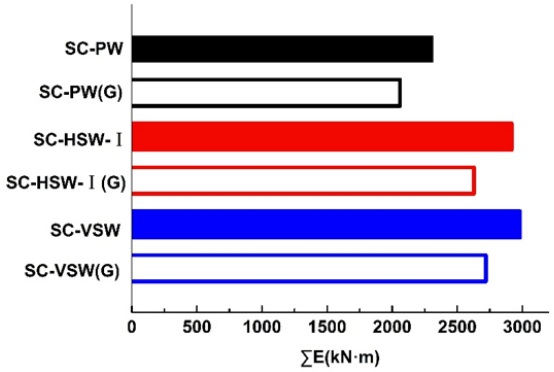

Figure 24: Accumulate energy dissipation of shear walls with and without gravity loads

Fig. 24 shows the accumulated energy dissipation of CoSPSWs and SPSWs with and without gravity load effects. Generally speaking, CoSPSWs still have higher accumulated energy dissipation than the SPSW with gravity loads, which is similar to the case without gravity loads. When gravity loads are applied, accumulated energy dissipation has decreased around 10% for the SPSW (SC-PW) and the CoSPSWs (SC-HSW-I, SC-VSW). It can be concluded that applying the gravity loads will will result in reduction of system energy dissipation, and it will affect these systems to a somewhat similar extent.

7. Conclusions

In this paper, nonlinear push-over analyses and cyclic analyses were conducted on Special Plate Shear Walls (SPSWs) and Corrugated Steel Plate Shear Walls (CoSPSWs), conclusions are drawn and shown as follows:

(1) Compared with plane SPSW, CoSPSW with deep corrugation has 34% higher initial stiffness, and 26% higher energy dissipation and 5% higher ultimate lateral strength; but CoSPSW with shallow corrugation has 25% lower ultimate lateral strength. Direction or configuration of the corrugation has very little influence on the cyclic behavior of CoSPSWs, especially when gravity loads are not applied.

(2) For CoSPSW with deep corrugation, the wall panel resists the lateral loads mainly through shear yielding, and the lateral strength is slightly higher than that of the SPSW. For CoSPSW with shallow corrugation, the wall panel resists the lateral loads through inelastic buckling and then incomplete tension field action. So the lateral strength is lower than that of the SPSW. Therefore, if system lateral strength is the main consideration during the design of a high-rise building, CoSPSW with deep corrugation will be recommended.

(3) When a weaker frame is used, tension field action of the SPSW cannot fully develop, which causes 18% and 25% reduction in the ultimate lateral strength and energy dissipation; CoSPSWs is less sensitive to the fame stiffness compared to the SPSW, especially the vertical CoSPSW.

(4) When gravity loads are applied, the ultimate lateral strength of the wall panels in the SPSW had a significant reduction of 38%; CoSPSWs is less sensitive to the gravity load effects compared to the SPSW.

Further experimental and analytical studies will be recommended to broaden the understanding of this type of new system and gain more insight into its seismic performance, such as failure modes of wall panels with different levels of corrugation, wall-frame interaction, multi-story CoSPSWs, and dynamic behavior of CoSPSWs, etc.

Acknowledgments

The authors gratefully acknowledge the financial supports for this research by the National Natural Science Foundation of China (grant number 91315301-03 and 51378340), the Specialized Research Fund for the Doctoral Program of Higher Education, China (grant number SRFDP: 20130032120055), and Program for New Century Excellent Talents in University (grant number NCET-13-0419)

References

Berman JW, Bruneau M. (2003). "Plastic analysis and design of steel plate shear wall." *Journal of Structural Engineering*, 129 (11) 1448-1456.

Berman JW, Bruneau M. (2005). "Experimental investigation of light-gauge steel plate shear walls." *Journal of Structural Engineering*, 131 (2) 259-267.

Borello DJ, Fahnestock LA. (2014). "Seismic Design and Analysis of Steel Plate Shear Walls with Coupling." *Journal of Structural Engineering*, 139 (8) 1263-1273.

Botors,R.B.G. (2006). "Nonlinear Finite Element Analysis of Corrugated Steel Plate Shear Walls." *M.Sc. Dissertation. University of Calgary*, Alberta, Canada.

Briassoulis D. (1986). "Equivalent orthotropic properties of corrugated sheets." *Computers & Structures*, 23 (2) 129-138.

Caccese V, Elgaaly M, Chen R. (1993). "Experimental study of thin steel-plate shear walls under cyclic load". *Journal of Structural Engineering*, 119 (2) 573-88.

Clayton PM, Winkley TB, Berman JW, Lowes LN. (2012). "Experimental Investigation of Self-Centering Steel Plate Shear Walls." *Journal of Structural Engineering*, 138 (7) 952-960.

Driver RG, Abbas HH, Sause R. (2006). "Shear behavior of corrugated web bridge girders." *Journal of Structural Engineering*, 132 (2) 195-203.

Driver RG, Kulak GL, Elwi AE,Laurie Kennedy DJ. (1998). "FE models of steel plate shear wall." *Journal of Structural Engineering*, 124 (2) 121-130.

Easley JT, McFarland DE. (1969). "Buckling of light-gauge corrugated metal shear diaphragms." *Journal of the Structural Division*, 95 (ST7) 1497-1516.

Egorova N, Eatherton M R, Maurya A. (2014). "Experimental study of ring-shaped steel plate shear walls." *Journal of Constructional Steel Research*, 103 179-189.

Eldib MEAH. (2009). "Shear buckling strength and design of curved corrugated steel webs for bridges." *Journal of Constructional Steel Research*, 65 (5) 2129-2139.

Emami F, Mofid M, Vafai A. (2013). "Experimental study on cyclic behavior of trapezoidally corrugated steel shear walls." *Engineering Structures*, 48 (48) 750-762.

Guo YL, Zhang QL, Wang XA. (2010). "A theoretical and experimental study of the shear strength of H-Shaped members with sinusoidal corrugated webs." *China Civil Engineering Journal*, 43 (10) 45-52 [in Chinese].

Hong-Gun Park, Jae-Hyuk Kwack, Sang-Woo Jeon. (2007). "Framed Steel Plate Wall Behavior under Cyclic Lateral Loading." *Journal of Structural Engineering*, 133 (3) 378-388.

Leiva-Aravena, L. (1987). "Trapezoidally Corrugated Panels-Buckling behavior Under Axial Pressure and Shear." *Division of Steel and Timber Structures*, 87-91.

Nie JG, Zhu L, Tao MX, Tang L. (2013). "Shear strength of trapezoidal corrugated steel webs." *Journal of Constructional Steel Research*, 85 105-115.

Tsai K C, Li C H, Lin C H, et al. (2010). “Cyclic Tests Of Four Two-Story Narrow Steel Plate Shear Walls-Part 1: Analytical Studies And Specimen Design.” *Earthquake Engineering and Structural Dynamics*, 39 (7) 775–799.

Tsai K C, Li C H, Lin C H, et al. (2010). “Cyclic Tests Of Four Two-Story Narrow Steel Plate Shear Walls-Part 2: Experimental results and design implications.” *Earthquake Engineering and Structural Dynamics*, 39 (7) 801-826.

Sabelli R, Bruneau M. (2006). “Steel plate shear walls. Steel design guide 20.” Chicago, IL, *American Institute of Steel Construction*.

Yi J, Gil H, Youm K, Lee HE. (2008). “Interactive shear buckling behavior of trapezoidally corrugated steel webs.” *Engineering Structures*, 30 (6) 1659-1666.

Zhao QH and Astaneh-Asl A. (2007). “Seismic Behavior of Steel Shear Wall Systems and Application of Smart Structures Technology.” *International Journal of Steel Structures*, 7 (1) 61-68.